

## *Supporting information*

### **Elucidating Facet-Dependent Hydrogenation Mechanism of Black-TiO<sub>2</sub> Through in situ Characterization**

*Bingyan Liu<sup>a,b</sup>, Tianfeng Duan<sup>b</sup>, Songhao Guo<sup>b,c</sup>, Kejun Bu<sup>b</sup>, Yiming Wang<sup>b</sup>, Jiabing Luo<sup>a</sup>,  
Mei Li<sup>b</sup>, Hongliang Dong<sup>b</sup>, Jun Zhang<sup>\*a</sup>, and Xujie Lü<sup>\*b</sup>*

<sup>a</sup> School of Materials Science and Engineering, China University of Petroleum (East China),  
Qingdao, 266580, China

<sup>b</sup> Center for High Pressure Science and Technology Advanced Research (HPSTAR),  
Shanghai 201203, China

<sup>c</sup> Center of Micro-Nano System, School of Information Science and Technology, Fudan  
University, Shanghai 200433, China

Email: [zhangji@upc.edu.cn](mailto:zhangji@upc.edu.cn) (J. Zhang); [xujie.lu@hpstar.ac.cn](mailto:xujie.lu@hpstar.ac.cn) (X. Lü)

## 1. Experimental section

**Synthesis of (101)-TiO<sub>2</sub>:** TiO<sub>2</sub> nanoparticles with exposed (101) facets were synthesized by a previously reported two-step hydrothermal method. In the first step, 0.3 g TiO<sub>2</sub> nanoparticles (anatase, 25 nm) were hydrothermally treated with 35 mL of KOH solution (10 M) in a Teflon autoclave with a capacity of 50 mL at 200 °C for 24 h. The resulting precipitate was washed with deionized water and an aqueous acetic acid solution until the pH=7.0. Then white powder was dried at 80 °C and the dried titanate nanowires (100 mg) were stirred in deionized water (60 mL) and heated in a Teflon autoclave (100 mL) at 200 °C for 24 h. The white precipitate was centrifuged and dried at 80 °C.

**Synthesis of (100)-TiO<sub>2</sub>:** Anatase TiO<sub>2</sub> nanobelts were synthesized *via* a two-step hydrothermal method described by Wong. In the first step, 0.3 g commercial anatase TiO<sub>2</sub> was stirred in a solution of 10 M NaOH prepared by solid NaOH (8 g) dissolved in deionized water (20 mL). The mixture was transferred to a 50 mL Teflon autoclave and heated at 200 °C for 24 h. The resulting Na<sub>1-x</sub>H<sub>x</sub>TiO<sub>3</sub> was washed with deionized water until the pH = 10.5 and then dried at 80 °C. Then 0.1 g of white precipitates was added into 40 mL deionized water and stirred for 30 min. The mixture was transferred to a 100 mL Teflon autoclave and heated at 200 °C for 24 h. Then the sample was centrifuged and dried at 80 °C.

**Synthesis of (001)-TiO<sub>2</sub>:** 25 mL of Titanium (IV) butoxide and 4 mL of hydrofluoric acid solution were injected in a 100 mL dried Teflon autoclave. Then held at 200 °C for 24 h. The white powder was separated by high-speed centrifugation and washed with ethanol and ultrapure water several times. The powders were soaked in a NaOH (0.1 M, 100 mL) solution to remove fluorine ions, followed by rinsing with ultrapure water five times. The white precipitate was centrifuged and dried at 120 °C.

### Hydrogen- and argon-treated TiO<sub>2</sub> nanocrystal samples

Initially, 10 mg of TiO<sub>2</sub> nanocrystal samples were weighed and compressed in a pellet mold under 1-ton pressure to ensure uniform densification across three distinct exposed-facet configurations. Following compression, samples were precision-sectioned and collectively mounted in a 400- $\mu$ m-diameter chamber. The chamber was pressurized with H<sub>2</sub> (or Ar) to 1.5 GPa, after which the samples were thermally treated at 200°C for 9 days under sustained pressure. Throughout the heating phase, time-resolved absorption spectroscopy and high-resolution optical imaging were systematically conducted on all specimens at 12-hour intervals.

### ***Characterization of the TiO<sub>2</sub> nanoparticles***

#### ***In situ* high-pressure characterizations**

The *in situ* high-pressure measurements of TiO<sub>2</sub> were performed by symmetric diamond anvil cells (DAC). Type II-a ultralow fluorescence diamonds with a culet size of 500  $\mu$ m were used to measure the UV-vis absorption spectroscopy and Raman spectra. A sample chamber was formed with a diameter of 400  $\mu$ m by laser-drilling the center part of stainless-steel gasket. The TiO<sub>2</sub> powders were loaded together into the sample chamber which was filled with pressure transition medium (hydrogen). Ruby balls were loaded in the chamber for the pressure calculation using the ruby fluorescence method.<sup>1</sup>

#### **Phase and Morphological Characterization**

Pre-hydrogenation samples were analyzed by powder X-ray diffraction (XRD, PANalytical X'Pert PRO MPD) with Cu K $\alpha$  radiation ( $\lambda$ =1.54056 Å). Post-hydrogenation structural evolution was probed via synchrotron radiation XRD at Shanghai Synchrotron Radiation Facility BL17B beamline ( $\lambda$ =0.68878 Å). Morphological transitions were systematically characterized using JEOL JEM-2100UHR TEM and FEI Versa 3D SEM, with identical imaging protocols applied to both pristine and hydrogenated specimens to ensure comparative validity.

### ***In situ* absorption measurements**

The UV-vis absorption spectra and optical images were measured by a home-designed spectroscopy system (Gora-UVN-FL, assembled by Ideaoptics, Shanghai, China). Absorption spectra were collected using a Xeon light source between 380 nm and 1100 nm.

### ***In situ* structural characterizations**

*In situ* Raman spectra were collected in the range of 100-900 cm<sup>-1</sup> by Renishaw Raman microscope. A laser excitation wavelength of 532 nm was utilized.

### **Electrical transport and photocurrent measurement**

The resistance of black-TiO<sub>2</sub> nanocrystals were determined using a Keithley 4200A semiconductor characterization system. NaCl powders were used as the pressure-transmitting medium. The temperature variation of the resistance was measured by using the liquid nitrogen cooling system and collected on Keithley 6200/2182A. The photocurrent measurement was collected by the Keithley 4200A semiconductor characterization system, and a xenon lamp was chosen as the light source.

Responsivity (R) is a critical parameter that characterizes the efficiency of photoelectric materials in converting incident optical power into electrical signals. It is defined as<sup>2</sup>:

$$R = \frac{I_{ph}}{P_{in} \cdot S}$$

where  $I_{ph} = I_{light} - I_{dark}$  denotes the photocurrent,  $I_{light}$  and  $I_{dark}$  represent the total current under illumination and the dark current, respectively.  $P_{in}$  refers to the incident light power density (25 mW/cm<sup>2</sup>), and  $S$  corresponds to the effective area of the hydrogenated TiO<sub>2</sub> nanocrystal samples ( $3.2 \times 10^{-5}$  cm<sup>2</sup>).

### **First-principles calculations**

Density functional theory (DFT)<sup>3, 4</sup> were performed using the Vienna *ab initio*

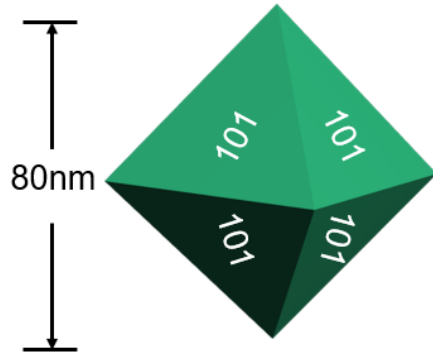
Simulation Package (VASP)<sup>5, 6</sup> with the projector augmented wave (PAW) method.<sup>7, 8</sup> The Perdew-Burke-Ernzerhof (PBE) functional described exchange-correlation interactions. Valence electronic for titanium ( $3s^2 3p^6 3d^3 4s^1$ ) and oxygen ( $2s^2 2p^4$ ) were explicitly. A 600-eV plane-wave cutoff and  $\Gamma$ -centered Monkhorst-Pack  $k$ -grids ( $0.2 \text{ \AA}^{-1}$  spacing) were applied. Convergence criteria were set to  $1.0 \times 10^{-6}$  eV (electronic) and  $1.0 \times 10^{-2}$  eV/ $\text{\AA}$  (ionic forces).

## 2. Determination of the specific surface area (SSA) and the percentage of the predominant facet

The specific calculation formulas are shown below.<sup>9, 10</sup>

$$SSA = \frac{\text{Total surface area}}{\text{Unit mass}} = \frac{S_{total}}{m} = \frac{S_{total}}{V \cdot \rho}$$

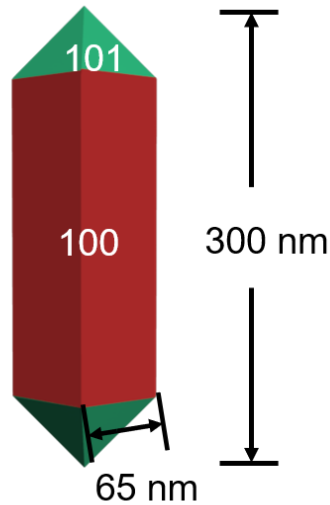
$$\rho = 3.9 \text{ g/cm}^3$$



Scheme 1 Schematic structure of (101)-TiO<sub>2</sub> sample

$$SSA_{101} = \frac{8 \times \frac{1}{2} \times \frac{40 \times 2}{\tan(68.3)} \times \frac{40}{\sin(68.3)} \times 10^{-18} \text{ m}^2}{2 \times \frac{1}{3} \times \left( \frac{40 \times 2}{\tan(68.3)} \right)^2 \times 40 \times 10^{-27} \times 3.9 \times 10^6 \text{ g}} = 52.01 \text{ m}^2/\text{g}$$

The (101) -TiO<sub>2</sub> NPs have an octahedral geometry with nearly 100% exposure of the (101) facet of TiO<sub>2</sub>. As shown in Scheme 1,  $S_{101} \approx 100\%$



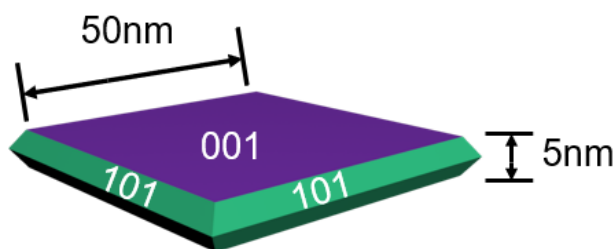
Scheme 2 Schematic structure of (100)-TiO<sub>2</sub> sample

As shown in Figures 1b, S2, the (100)-TiO<sub>2</sub> HRTEM images confirm the predominant facet is (100) and the side facet is (101), which agrees well with previous report.<sup>9, 11</sup> The nanorods have an average length of 300 nm and thickness of 65 nm. The calculation for the SSA and the percentage of (100) facets ( $SSA_{100}$  and  $S_{100}$ ) is shown below.

$$\begin{aligned}
 & SSA_{100} \\
 &= \frac{8 \times \frac{1}{2} \times 65 \times \frac{65}{2 \times \cos(68.3)} + 4 \times 65 \times (300 - 2 \times \frac{65}{2 \times \tan(68.3)}) \times 10^{-18} \text{ m}^2}{2 \times \frac{1}{3} \times \left[ 65^2 \times \frac{65}{2 \times \tan(68.3)} - 65^2 \times (300 - 2 \times \frac{65}{2 \times \tan(68.3)}) \right] \times 3.9 \times 10^{-21} \text{ g}} \\
 &= 20.20 \text{ m}^2/\text{g}
 \end{aligned}$$

$$S_{100} = \frac{\text{Area of (100) facets}}{\text{Total surface area}}$$

$$= \frac{4 \times 65 \times \left( 300 - 2 \times \frac{65}{2 \times \tan(68.3)} \right)}{8 \times \frac{1}{2} \times 65 \times \frac{65}{2 \times \cos(68.3)} + 4 \times 65 \times \left( 300 - 2 \times \frac{65}{2 \times \tan(68.3)} \right)} = 76\%$$



Scheme 3 Schematic structure of (001)-TiO<sub>2</sub> sample

The (001) -TiO<sub>2</sub> NPs have a plate-like morphology with an average edge length of 50 nm and thickness of 5 nm and the schematic structure is shown below. On the basis of a previous report, the percentage of the predominant (001) facet ( $S_{001}$ ) is given according to equation shown below, where  $\theta$ ,  $a$ ,  $h$  represents the angle between the (101) and (001) facets of anatase (68.3°), the length of (001) facet, and the thickness of nanoplate, respectively.<sup>12</sup>

$$SSA_{001} = \frac{50 \times 50 \times 2 + 8 \times \frac{1}{2} \times (50 + 50 + \frac{2.5 \times 2}{\tan(68.3)}) \times \frac{2.5}{\sin(68.3)} \times 10^{-18} \text{ m}^2}{2 \times \frac{1}{3} \times \left[ (50 + \frac{2.5 \times 2}{\tan(68.3)})^3 \times \frac{1}{2} - (50)^3 \times \frac{1}{2} \right] \times \tan(68.3) \times 3.9 \times 10^{-21} \text{ g}}$$

$$= 80.15 \text{ m}^2/\text{g}$$

$$S_{001} = \frac{\cos(\theta)}{\cos(\theta) + \left[ \frac{a}{a + \frac{h}{\tan(\theta)}} \right]^{-2} - 1}$$

$$S_{001} = \frac{\cos(68.3)}{\cos(68.3) + \left[ \frac{50}{50 + \frac{5}{\tan(68.3)}} \right]^{-2} - 1} = 82\%$$



## Supplementary figures

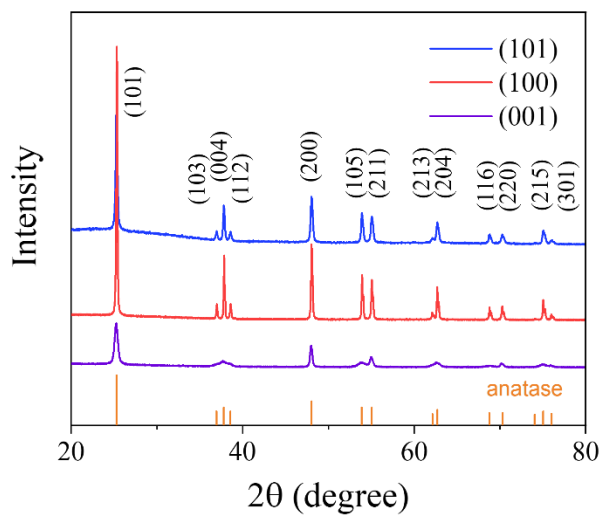


**Fig. S1.** XRD spectra of the TiO<sub>2</sub> with different exposed surface terminations.

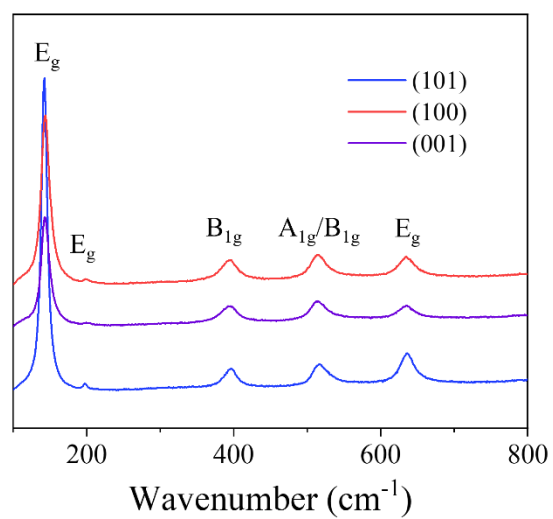


**Fig. S2.** Raman spectra of the TiO<sub>2</sub> with different exposed surface terminations.

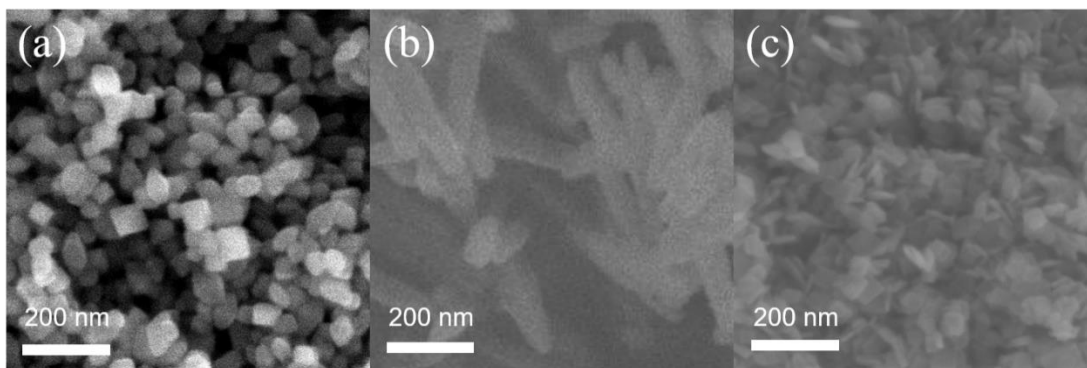


**Fig. S3.** SEM images of the  $\text{TiO}_2$  with different exposed surface terminations. (a) (101)- $\text{TiO}_2$  (b) (100)- $\text{TiO}_2$  (c) (001)- $\text{TiO}_2$ .

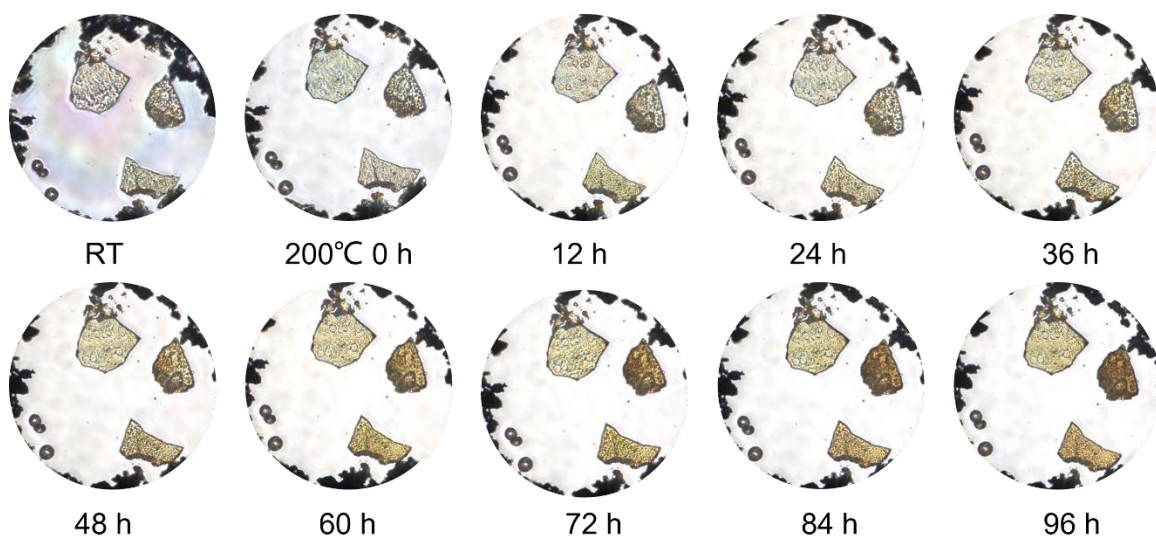


**Fig. S4.** The optical images of three  $\text{TiO}_2$  samples heated at 200 °C over time.

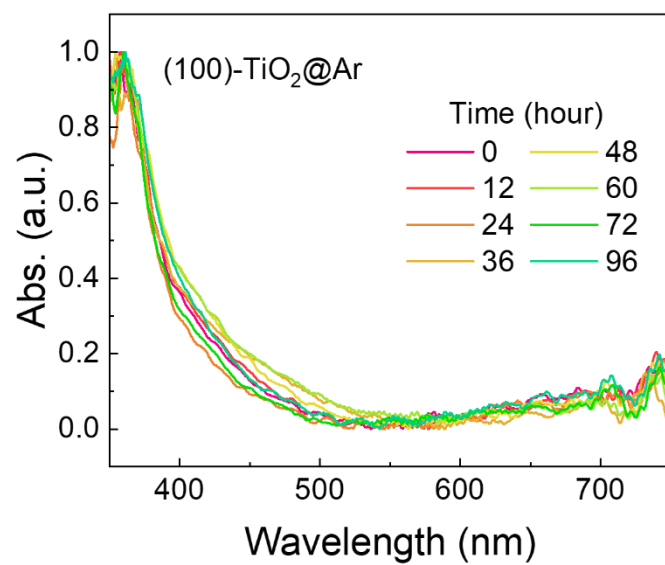


**Fig. S5.** UV-vis absorption spectra of the TiO<sub>2</sub>@Ar heated at 200 °C over time.

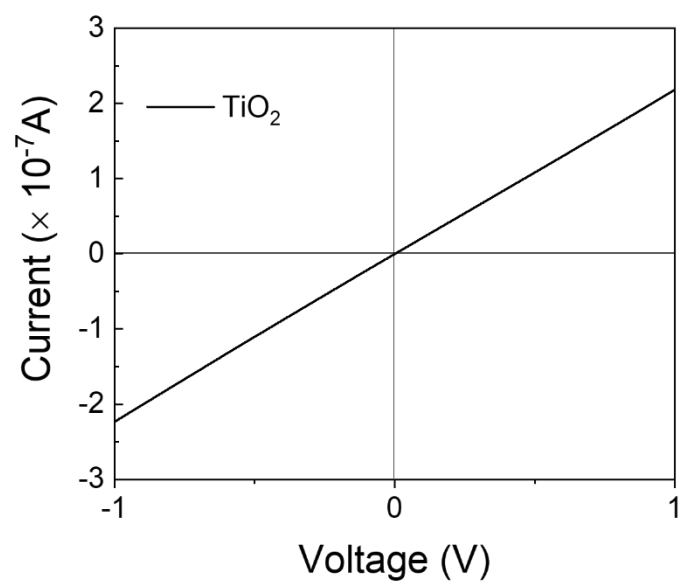


**Fig. S6.** I-V curve of the pristine TiO<sub>2</sub> nanocrystals.

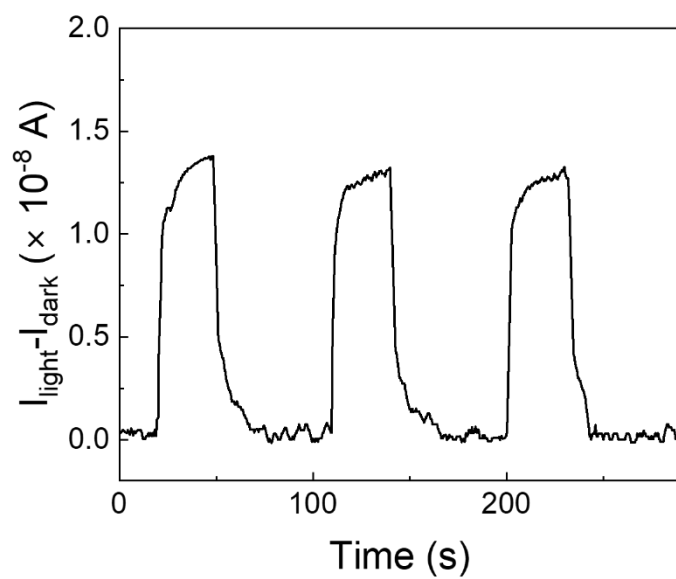


**Fig. S7.** Photo-response of the pristine TiO<sub>2</sub> nanocrystals measured at a bias of 0.1 V.

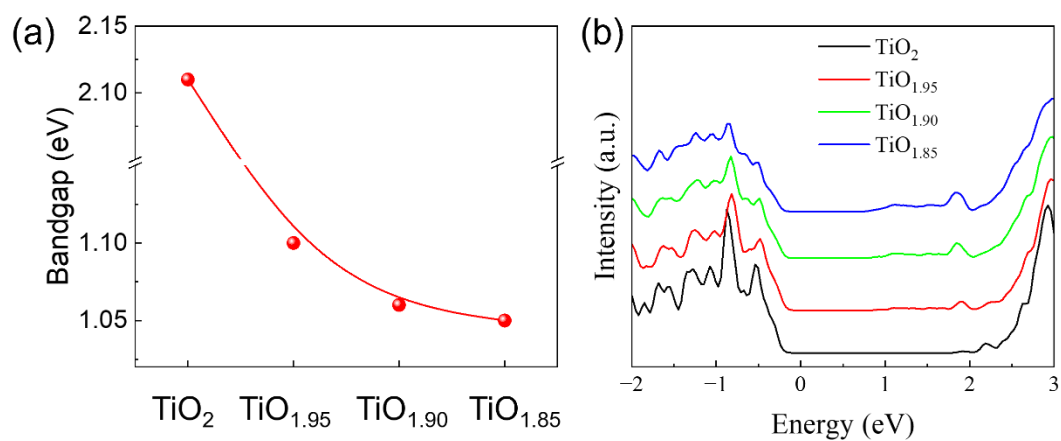


**Fig. S8.** Calculated (a) bandgap and (b) DOS of TiO<sub>2-x</sub> samples with different oxygen vacancy concentrations



## References

- 1 H. K. X. Mao, J.; Bell, P. M., *J. Geophys. Res.*, 1986, **91**, 4673-4676.
- 2 H. Feng, G. Zhang, Z. Feng, Q. Li, G. Wang, Y. Li, Y. Fang and C. Liu, *Appl. Phys. Lett.*, 2024, **124**, 043902.
- 3 P. Hohenberg and W. Kohn, *Physical Review*, 1964, **136**, B864-B871.
- 4 W. Kohn and L. J. Sham, *Physical Review*, 1965, **140**, A1133-A1138.
- 5 G. Kresse and J. Furthmüller, *Comput. Mater. Sci*, 1996, **6**, 15-50.
- 6 G. Kresse and J. Furthmüller, *Phys. Rev. B*, 1996, **54**, 11169-11186.
- 7 P. E. Blöchl, *Phys. Rev. B*, 1994, **50**, 17953-17979.
- 8 G. Kresse and D. Joubert, *Phys. Rev. B*, 1999, **59**, 1758-1775.
- 9 C. Li, C. Koenigsmann, W. Ding, B. Rudshiteyn, K. R. Yang, K. P. Regan, S. J. Konezny, V. S. Batista, G. W. Brudvig, C. A. Schmittenmaer and J. H. Kim, *J. Am. Chem. Soc.*, 2015, **137**, 1520-1529.
- 10 M. Chen, J. Ma, B. Zhang, F. Wang, Y. Li, C. Zhang and H. He, *Appl. Catal., B*, 2018, **223**, 209-215.
- 11 J. Li and D. Xu, *Chem. Commun.*, 2010, **46**, 2301-2303.
- 12 X. Han, Q. Kuang, M. Jin, Z. Xie and L. Zheng, *J. Am. Chem. Soc.*, 2009, **131**, 3152–3153.